

## Observation of Acceleration of HI Clouds Within the Fermi Bubbles

FELIX J. LOCKMAN,<sup>1</sup> ENRICO M. DI TEODORO,<sup>2</sup> AND N. M. MCCLURE-GRIFFITHS<sup>2</sup>

<sup>1</sup>*Green Bank Observatory, Green Bank, WV 24944, USA*

<sup>2</sup>*Research School of Astronomy and Astrophysics - The Australian National University, Canberra, ACT, 2611, Australia*

### ABSTRACT

The  $\sim 200$  HI clouds observed to be entrained in the Fermi Bubble wind show a trend of increasing maximum  $|V_{\text{LSR}}|$  with Galactic latitude. We analyze previous observations and present new data from the Green Bank Telescope that rule out systematic effects as the source of this phenomenon. Instead, it is likely evidence for acceleration of the clouds. The data suggest that clouds in the lower 2 kpc of the Fermi Bubbles, within the Bubble boundaries established from X-ray studies, have an outflow velocity that rises from  $\approx 150 - 200 \text{ km s}^{-1}$  close to the Galactic Center and reaches  $\approx 330 \text{ km s}^{-1}$  at a distance of  $2.5 - 3.5 \text{ kpc}$ . These parameters are also consistent with the kinematics of UV absorption lines from highly ionized species observed against two targets behind the Fermi Bubbles at  $b = -6^\circ 6'$  and  $b = +11^\circ 2'$ . The implied neutral cloud lifetime is  $4 - 10 \text{ Myr}$ .

*Keywords:* Galaxy: center – Galaxy: nucleus – ISM: clouds – ISM: jets and outflows – ISM: kinematics and dynamics

### 1. INTRODUCTION

Energetic processes in the center of the Milky Way, arising from either star formation or active galactic nuclei (AGN) activity, have created two lobes extending to latitude  $|b| \approx 55^\circ$  above and below the Galactic Center. Although evidence for a nuclear wind was being discussed many years before the launch of the Fermi  $\gamma$ -ray telescope (e.g., Bland-Hawthorn & Cohen 2003; Veilleux et al. 2005; Keeney et al. 2006) the structures are now generally referred to as the Fermi Bubbles, clearly detected in  $\gamma$ -ray emission (Su et al. 2010). Nuclear winds are ubiquitous in star-forming galaxies (Veilleux et al. 2005), and the Fermi bubbles give us the opportunity to study this phenomenon at a level of detail not possible for more distant systems. Associated components are visible in broad-band emission across the electromagnetic spectrum (Dobler & Finkbeiner 2008; Kataoka et al. 2013; Carretti et al. 2013). The Bubbles are also coincident with a void in the extended Galactic neutral hydrogen (HI) layer at Galactocentric distances  $R \lesssim 2.4 \text{ kpc}$  (Lockman 1984; Lockman & McClure-Griffiths 2016).

Spectroscopic observations of 21cm HI emission have detected material entrained in the bubbles at radial velocities exceeding  $300 \text{ km s}^{-1}$  (McClure-Griffiths et al. 2013; Di Teodoro et al. 2018) and measurements of ultraviolet (UV) absorption lines along paths through the bubbles reveal hot gas at similar large non-circular velocities in many stages of ionization (Fox et al. 2015; Savage et al. 2017). Within  $|b| \lesssim 11^\circ$  of the Galactic plane the 21cm and UV spectra have similar kinematics and have been modeled by a symmetric biconical outflow with constant velocity  $V_{\text{out}} \simeq 330 \text{ km s}^{-1}$  through an opening angle of  $140^\circ$  centered on the Galactic Center (Di Teodoro et al. 2018). In this paper we show evidence from the 21cm HI surveys that neutral clouds entrained in the Fermi Bubble wind appear to be accelerating from velocities near  $150 \text{ km s}^{-1}$  close to the Galactic Center to  $330 \text{ km s}^{-1}$  at a distance of several kpc.

The paper is organized as follows. In Section 2 we describe 21cm HI and UV spectra of gas entrained in the Fermi Bubble wind and present new observations made with the Green Bank Telescope (GBT). These data reveal a kinematic anomaly in the form of an absence of gas at  $|V_{\text{LSR}}| > 200 \text{ km s}^{-1}$  within  $4^\circ$  of the Galactic plane. Section 3 compares the observed distribution of velocities with that expected from a constant-velocity nuclear wind and concludes that there is a discrepancy. Section 4 considers a set of possible systematic effects

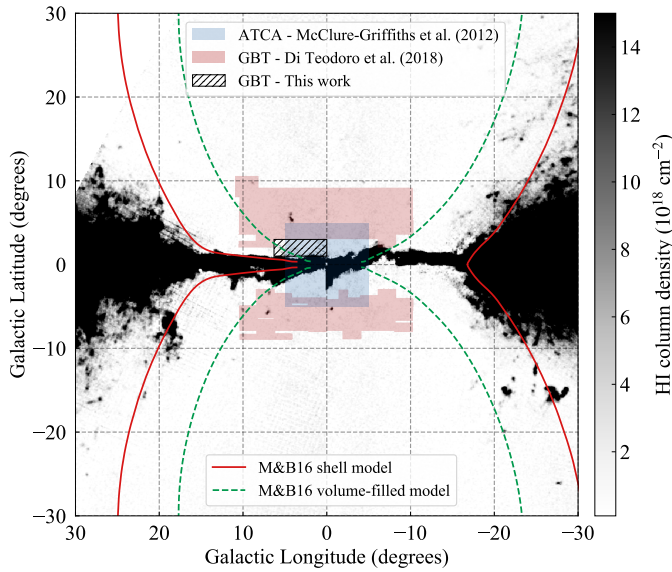


**Figure 1.** The greyscale is proportional to the HI column density at the Galactic tangent points where  $R = R_0 \sin(\ell)$  (Lockman & McClure-Griffiths 2016). The red solid curves and the green dashed curves mark the shell and volume-filled regions of the Fermi bubble from the model of Miller & Bregman (2016) derived from X-ray emission. Hot, shocked wind material lies within the volume marked by the dashed green curves, while the outer shell includes shocked interstellar and circumgalactic material. The area studied in the ATCA survey (McClure-Griffiths et al. 2013) is marked by a rectangle  $10^\circ \times 10^\circ$  around the Galactic Center, while the other shaded areas above and below mark regions covered in the GBT survey (DiT18), and the new observations presented here (crosshatched region).

that might produce the kinematic anomaly and concludes that the anomaly is real. Section 5 presents a simulation that matches the observed kinematics when clouds are constantly accelerated for the first few kpc away from the Galactic Center. The paper concludes with a discussion in Section 6.

## 2. GAS ENTRAINED IN THE FERMI BUBBLES

Figure 1 shows the HI emission along the tangent points of the Milky Way from Lockman & McClure-Griffiths (2016) and superimposed on it the shell (red line) and volume-filled (green-dashed line) models for the Fermi Bubble X-ray emission (Miller & Bregman 2016). The  $10^\circ \times 10^\circ$  box centered on the Galactic Center (pink shaded) marks the region surveyed in HI by the Australia Telescope Compact Array (ATCA) which first detected 86 HI clouds entrained in the Fermi Bubble wind (McClure-Griffiths et al. 2013, hereafter McG13). The red-shaded larger irregular boxes farther from the plane mark the regions surveyed by the Green Bank Telescope (GBT) which detected an additional 106

clouds (Di Teodoro et al. 2018, hereafter DiT18). Table 1 compares the properties of those two radio HI surveys (columns 2 and 4). Note that column density  $N_{\text{HI}}$  used here always refers to the average over the resolution element of the observation.

When all observational effects are taken into account, the neutral cloud population entrained in the Fermi Bubbles is nearly symmetric with respect to Galactic latitude, Galactic longitude, and  $V_{\text{LSR}}$ , and can be modelled as arising from a filled bi-symmetric cone with only two free parameters: a maximum opening angle  $\alpha$ , and a constant radial outflow velocity  $V_{\text{out}}$  (see DiT18, for details). The outflowing gas clouds must be distributed throughout the cones, because the HI clouds in any area (and the ionized components observed in UV absorption) span a range of velocity implying a range of ejection angle  $\phi$ , where  $\phi$  is measured from the plane in the vertical direction. The gas we observe is presumably entrained in a much faster hot wind whose kinematic structure is not observable.

The HI clouds are detected down to a  $|V_{\text{LSR}}|$  limited by confusion with unrelated lower-velocity HI emission. In practice, the lower limit on  $|V_{\text{LSR}}|$  of detectable HI clouds is set by the sensitivity of the data and the algorithms used to identify and measure the clouds, which differ between McG13 and DiT18. Generally speaking, measurable cloud velocities are limited to  $|V_{\text{LSR}}| \gtrsim 50 \text{ km s}^{-1}$  for the ATCA data and  $\gtrsim 75 \text{ km s}^{-1}$  for the GBT. This issue of confusion will be discussed further in Section 4.1.

McG13 fitted a kinematic model to the ATCA data, and DiT18 modelled the GBT data. Both the ATCA and GBT cloud samples are consistent with a cone opening angle  $\alpha \approx 140^\circ$ , but analysis of the lower  $|b|$  ATCA survey found  $V_{\text{out}} = 220 \text{ km s}^{-1}$  while the GBT data required a model with a significantly higher  $V_{\text{out}} = 330 \text{ km s}^{-1}$ .

The reason for the difference is clear from Figure 2. The left panel shows the  $|V_{\text{LSR}}|$  for the combined ATCA and GBT samples plotted against the absolute value of the Galactic latitude,  $|b|$ . Dotted and dashed lines show the positive and negative  $V_{\text{LSR}}$  limits of the ATCA survey over its latitude range. The GBT survey covered  $\pm 670 \text{ km s}^{-1}$ . It is evident that the maximum  $|V_{\text{LSR}}|$  rises from about  $125 \text{ km s}^{-1}$  at  $|b| \sim 1^\circ$ , the smallest latitudes where discrete clouds have been detected, to  $\sim 300 \text{ km s}^{-1}$  around  $|b| = 5^\circ$ . The ATCA survey over  $|b| \leq 5^\circ$  did not detect any HI clouds with  $|V_{\text{LSR}}| > 210 \text{ km s}^{-1}$  although this velocity range was included in its spectral coverage, while the higher-latitude GBT survey found clouds with  $|V_{\text{LSR}}| \gtrsim 330 \text{ km s}^{-1}$ . We refer to this difference as the kinematic anomaly.

**Table 1.** Properties of Galactic Center HI surveys used in this work.

Property	ATCA <sup>1</sup>	GASS <sup>2</sup>	GBT <sup>3</sup>	new GBT <sup>4</sup>
Angular Resolution	2'4	16'2	9'5	9'1
Longitude range	$\pm 5^\circ$	$\pm 12^\circ$	$\pm 10^\circ$	$0^\circ - 6^\circ$
Latitude range	$\pm 5^\circ$	$\pm 12^\circ$	$-8^\circ \lesssim b \lesssim -4^\circ$ $+3^\circ \lesssim b \lesssim +9^\circ$	$1^\circ - 3^\circ$
Velocity range LSR ( $\text{km s}^{-1}$ )	$-309 < V_{\text{LSR}} < +349$	$\pm 470$	$\pm 670$	$\pm 656$
Noise rms $\sigma_{T_b}$ (mK) <sup>a</sup>	700	57	30 <sup>b</sup>	35
$N_{\text{HI}}$ lower limit ( $\text{cm}^{-2}$ ) <sup>c</sup>	$2.1 \times 10^{19}$	$1.6 \times 10^{18}$	$9.0 \times 10^{17}$	$1.0 \times 10^{18}$

<sup>1</sup>McClure-Griffiths et al. (2013); <sup>2</sup>McClure-Griffiths et al. (2009); <sup>3</sup>Di Teodoro et al. (2018); <sup>4</sup>This work.

<sup>a</sup>In a  $1 \text{ km s}^{-1}$  channel.

<sup>b</sup>The range is 23 mK to 40 mK over the mapped area.

<sup>c</sup>Averaged over a resolution element for a Gaussian line with amplitude  $A = 3\sigma_{T_b}$  and FWHM =  $30 \text{ km s}^{-1}$ .

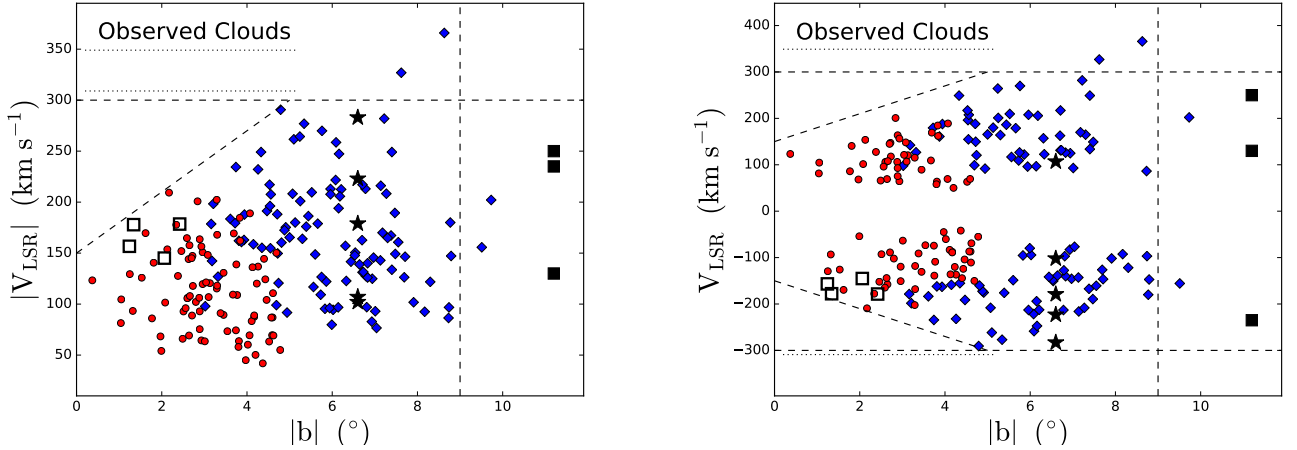


**Figure 2.** *Left panel:* the  $|V_{\text{LSR}}|$  of clouds detected in the ATCA survey (McG13; red circles) and the GBT survey (DiT18; blue diamonds) as a function of the absolute value of the Galactic latitude,  $|b|$ . Dotted lines show the negative and positive  $|V_{\text{LSR}}|$  limits, respectively, of the ATCA survey over its latitude range. The GBT survey is complete to  $\pm 670 \text{ km s}^{-1}$ . Stars show velocities of five high-velocity UV absorption line components detected towards a distant star behind the Fermi Bubble at  $(\ell, b) = (1^\circ 67, -6^\circ 63)$  (Savage et al. 2017), while filled rectangles show the three high-velocity UV absorption components detected toward an AGN at  $(\ell, b) = (10^\circ 4, +11^\circ 2)$  from Fox et al. (2015). Open rectangles mark clouds discovered in the new GBT data described in this paper. Fiducial dashed lines at  $300 \text{ km s}^{-1}$ , and from  $150 \text{ km s}^{-1}$  at  $|b| = 0^\circ$  to  $300 \text{ km s}^{-1}$  at  $|b| = 5^\circ$ , outline the region where clouds should be detected from a constant  $V_{\text{out}} = 330 \text{ km s}^{-1}$  wind, but are not. This defines the kinematic anomaly. At positive latitudes the GBT survey is complete at  $b \leq +9^\circ$  (dashed vertical line). At negative latitudes the survey is complete to only  $b \geq -8^\circ$ . *Right panel:* Same as left panel, but for positive and negative velocities separately, and a line from  $-150 \text{ km s}^{-1}$  to  $-300 \text{ km s}^{-1}$ . The anomaly appears in both positive and negative velocity clouds.

The right panel of Figure 2 shows the HI clouds plotted separately for negative and positive  $V_{\text{LSR}}$ . The absence of clouds at  $|V_{\text{LSR}}| > 200 \text{ km s}^{-1}$  near the Galactic plane appears for both approaching and receding clouds.

### 2.1. UV Absorption Spectroscopy

Results from UV absorption line measurements on sightlines that pierce the Fermi Bubbles over these latitudes are included in Figure 2. The star LS 4825, a B1 Ib-II star located  $21 \pm 5 \text{ kpc}$  from the Sun at  $(\ell, b) = (1^\circ 67, -6^\circ 63)$  shows discrete absorption features between velocities  $-283 \text{ km s}^{-1}$  and  $+107 \text{ km s}^{-1}$  over a range of species and ionization states, including Si III, C IV, Si IV, and N V (Savage et al. 2017). Above the plane, absorption spectra toward the AGN PDS 456 at  $(\ell, b) = (10^\circ 4, +11^\circ 2)$  shows UV metal-line absorption components (e.g., C II, S II, Si IV) from  $-235 \text{ km s}^{-1}$  to  $+250 \text{ km s}^{-1}$  (Fox et al. 2015). These absorption velocities are consistent with the velocity range of the HI clouds at a similar latitude.

Savage et al. (2017) note that the interstellar absorption toward a foreground star nearly aligned with LS 4825, but at a distance of only  $< 7 \pm 1.7 \text{ kpc}$ , is completely consistent with normal Galactic rotation, confirming that the high non-circular velocities arise in the Fermi Bubble and are not a general feature of the interstellar medium in the direction of the Galactic Center.

There are also measurements of high-velocity UV absorption lines through the Fermi Bubbles quite far from the Galactic Plane, at  $28^\circ 5 \leq |b| \leq 50^\circ 3$  (Bordoloi et al. 2017; Karim et al. 2018), but these are well away from the areas we consider here.

### 2.2. Additional 21cm HI Data

There are significant differences between the McG13 ATCA and DiT18 GBT surveys in sensitivity and angular resolution, as well as in the method of extracting clouds, which might be important when comparing population properties. For this reason we did a search for HI clouds in the GASS survey (McClure-Griffiths et al. 2009; Kalberla et al. 2010) which covers the entire area of Figure 1, and made new observations with the GBT over 12 square degrees that overlap part of the ATCA survey but with greater sensitivity. Parameters of the GASS and new GBT observations are given in columns 3 and 5 of Table 1. The GBT observations and data reduction are described in Appendix A.

No clouds were detected in the GASS data that had not already been included in the ATCA and GBT samples. In contrast, while the new GBT observations recovered all clouds seen in the ATCA survey in the same part of the sky, four new clouds were detected as well.

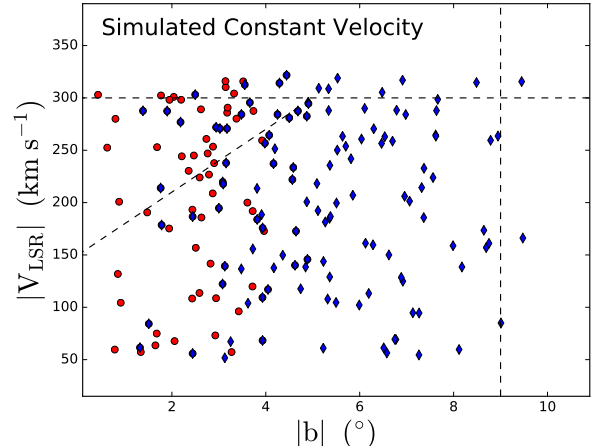


**Figure 3.**  $|V_{\text{LSR}}|$  vs.  $|b|$  for a simulated population of clouds filling two bicones with constant  $V_{\text{out}} = 330 \text{ km s}^{-1}$  and a maximum opening angle  $\alpha = 140^\circ$ , the properties from DiT18. Red circles show clouds that appear in the area covered only in the ATCA survey and blue diamonds show those that occur in regions covered by the GBT surveys. The dashed fiducial lines are identical to those in Fig. 2. This simulation does not match the observations as it produces many clouds with  $|V_{\text{LSR}}| > 200 \text{ km s}^{-1}$  at low latitudes that are not observed.

Their properties are listed in Table 2. The new GBT clouds have velocities in the range of those detected in the ATCA survey. These are shown as open rectangles in Figure 2 and do not resolve the kinematic anomaly. We conclude that the absence of HI clouds at the highest  $|V_{\text{LSR}}|$  at  $|b| \lesssim 4^\circ$  is not simply a result of different properties of the ATCA and GBT surveys.

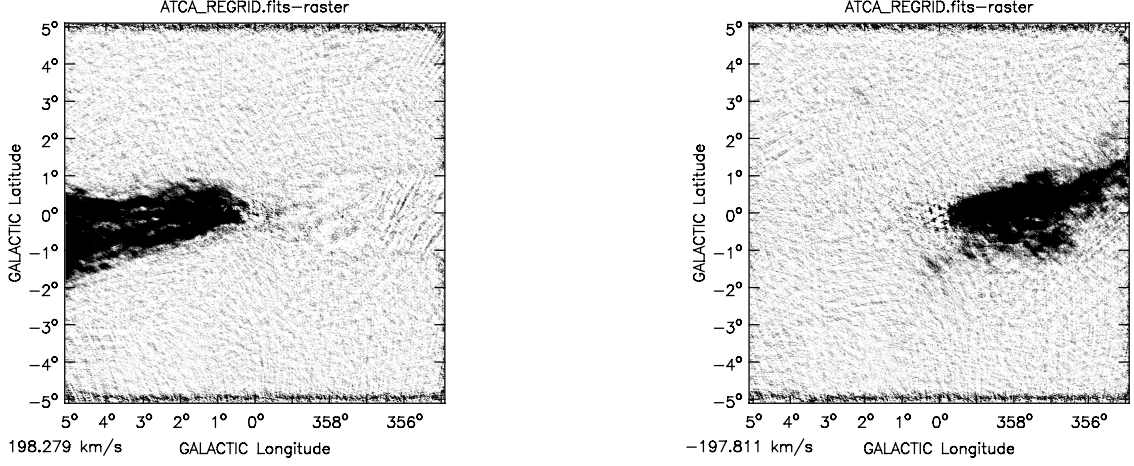
## 3. EXPECTATIONS FROM A CONSTANT VELOCITY WIND

Figure 3 shows the expected  $|V_{\text{LSR}}|$  vs.  $|b|$  for a population of clouds drawn from a random sample originating in a bi-cone centered on the Galactic Center with an opening angle  $\alpha = 140^\circ$  and a constant radial outflow velocity  $V_{\text{out}} = 330 \text{ km s}^{-1}$ , the parameters derived by DiT18, who analyzed only the GBT survey data. The dashed fiducial lines are identical to those in Figure 2 and show that these parameters are not a good description of the combined data set, as they predict a number of clouds with relatively high velocity at low latitude that are not present, especially in the ATCA data.

Before considering models incorporating acceleration, we examine the possibility that the kinematic anomaly arises from systematic effects.

## 4. POSSIBLE SYSTEMATIC EFFECTS

In this section we consider a number of systematic observational effects that might be related to the absence



**Figure 4.** ATCA HI survey data binned to  $3 \text{ km s}^{-1}$  at  $V_{\text{LSR}} = +198 \text{ km s}^{-1}$  (*left panel*) and  $V_{\text{LSR}} = -198 \text{ km s}^{-1}$  (*right panel*). At these velocities one still sees emission from the tilted nuclear disk, but it causes confusion over  $\lesssim 10\%$  of the area of the field. At higher  $|V_{\text{LSR}}|$  the confused region is correspondingly smaller. There are no selection effects preventing detection of HI clouds at  $|V_{\text{LSR}}| \geq 200 \text{ km s}^{-1}$  over  $\geq 90\%$  of the field.

**Table 2.** Clouds detected in the new GBT Observations. Columns as follow: (1) Cloud assigned name; (2) Galactic longitude; (3) Galactic latitude; (4) LSR velocity; (5) Line width FWHM; (6) Maximum line brightness temperature; (7) Maximum HI column density; (8) radius FWHM; (9) HI mass. Columns (2) and (3) are from a Gaussian fit of the integrated total spectrum. Column (7) is from columns (5) and (6). Columns (8)-(9) are calculated assuming a distance from the Sun of 8.5 kpc. Uncertainties are propagated from the errors associated with the Gaussian fits.

Name	$\ell$	$b$	$V_{\text{LSR}}$	FWHM	$T_{\text{b,max}}$	$N_{\text{HI,max}}$	$r$	$M_{\text{HI}}$
	( $^{\circ}$ )	( $^{\circ}$ )	( $\text{km s}^{-1}$ )	( $\text{km s}^{-1}$ )	(K)	( $10^{19} \text{ cm}^{-2}$ )	(pc)	( $M_{\odot}$ )
(1)	(2)	(3)	(4)	(5)	(6)	(7)	(8)	(9)
G1.43+2.42-176	1.43	2.42	$-176.4 \pm 0.8$	$31.0 \pm 1.8$	$0.18 \pm 0.01$	$1.1 \pm 0.1$	$19 \pm 4$	$140 \pm 43$
G1.60+2.06-147	1.60	2.06	$-147.2 \pm 0.7$	$24.3 \pm 1.7$	$0.28 \pm 0.02$	$1.3 \pm 0.1$	$23 \pm 2$	$250 \pm 38$
G1.78+1.34-177	1.78	1.34	$-177.4 \pm 0.4$	$19.4 \pm 0.9$	$0.37 \pm 0.02$	$1.4 \pm 0.1$	$26 \pm 2$	$340 \pm 43$
G4.34+1.24-157	4.34	1.24	$-157.4 \pm 0.5$	$25.2 \pm 1.2$	$0.24 \pm 0.01$	$1.2 \pm 0.1$	$32 \pm 3$	$426 \pm 63$



of clouds with  $|V_{\text{LSR}}| > 200 \text{ km s}^{-1}$  at  $|b| \lesssim 4^\circ$ , and conclude that none seems likely to account for the kinematic anomaly.

#### 4.1. Confusion

Clouds at low  $|V_{\text{LSR}}|$  can be blended with unrelated foreground emission and become difficult to distinguish. The velocity where this confusion sets in varies somewhat with latitude but typically occurs at  $|V_{\text{LSR}}| \lesssim 50 \text{ km s}^{-1}$ . In addition to confusion from foreground HI in the Galactic disk, there can be confusion from gas having non-circular motions associated with the inner Galaxy. The ATCA survey covered regions within a few degrees of the Galactic plane where the nuclear disk, 3-kpc arm, and other features with large non-circular velocities (e.g., Oort 1977; Burton & Liszt 1978; Binney et al. 1991) make it impossible to identify clouds associated with expansion of the Fermi Bubbles unambiguously. But this effect is limited.

Figure 4 shows channel maps for ATCA data at  $V_{\text{LSR}} = \pm 198 \text{ km s}^{-1}$ . Although within a few degrees of the Galactic plane there is significant emission at some longitudes,  $\approx 90\%$  of the field has no confusing emission preventing the detection of HI clouds at the given velocity. At ever larger  $|V_{\text{LSR}}|$  the confusing emission occupies an ever smaller area, reaching  $\approx 4\%$  at  $|V_{\text{LSR}}| = 250 \text{ km s}^{-1}$  and becoming negligible at  $|V_{\text{LSR}}| \geq 285 \text{ km s}^{-1}$  for both positive and negative velocities. We conclude that confusion has no more than a 10% effect on our ability to detect HI clouds at  $|V_{\text{LSR}}| \gtrsim 200 \text{ km s}^{-1}$  within  $5^\circ$  of the Galactic plane. In fact, confusion is actually less at  $|V_{\text{LSR}}| \gtrsim 200 \text{ km s}^{-1}$  than at velocities closer to zero, favoring detection of clouds with higher rather than lower  $|V_{\text{LSR}}|$ , exactly the opposite of the observed effect

#### 4.2. Sensitivity

The noise in a spectrum is a combination of contributions from instrumentation, thermal and non-thermal Galactic continuum emission, and at some velocities, emission from the HI line itself. The Earth’s atmosphere contributes a small bit as well. Because the HI clouds we study are detectable only at velocities lacking other bright HI emission, the only important sources of noise for this discussion are instrumental, atmospheric, and continuum emission. None of these components varies with frequency to an extent that would effect the detectability of HI at different velocities.

#### 4.3. Change in cloud detectability with $|V_{\text{LSR}}|$

The detectability of the clouds seen in the surveys depends mainly on their peak 21cm HI brightness temperature, which is shown for the GBT sample in Figure 5

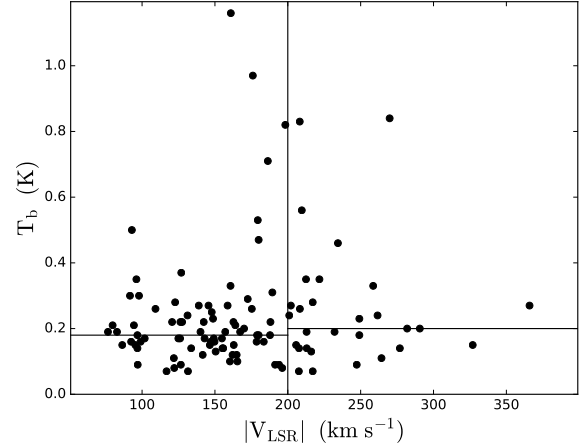


**Figure 5.** GBT cloud peak HI line brightness temperature,  $T_b$ , plotted against  $|V_{\text{LSR}}|$  for clouds from the DiT18 survey. Horizontal lines mark the median  $T_b$  for clouds with  $|V_{\text{LSR}}| < 200 \text{ km s}^{-1}$ , and  $|V_{\text{LSR}}| > 200 \text{ km s}^{-1}$ , respectively. There is no significant difference between the line brightness, and hence the detectability, of clouds in these two velocity ranges.

plotted against the  $|V_{\text{LSR}}|$ . Clouds to the right of the vertical line at  $200 \text{ km s}^{-1}$  have the large velocities that are not found at  $|b| \lesssim 4^\circ$  (Figure 2). The horizontal lines at 0.18 K and 0.20 K show the median HI line brightness temperature of clouds with  $|V_{\text{LSR}}|$  greater than and less than  $200 \text{ km s}^{-1}$ , respectively. There is no significant difference in the median peak line temperature, hence the detectability, of higher-velocity clouds compared to those at lower velocity. This conclusion also holds for the mean of the cloud line brightness temperature. We conclude that there is no evidence of a change in cloud detectability with  $|V_{\text{LSR}}|$  that could produce the kinematic anomaly observed in Figure 2.

## 5. ACCELERATION OF HI CLOUDS?

To explore the kinematics of the Fermi Bubble clouds we simulate a distribution of clouds within the confines of the Miller & Bregman (2016) shell model whose projected outlines are shown in Figure 1. In a right-handed cylindrical coordinate system, position is given by  $(R, \theta, z)$  centered on the Galactic Center, where the Sun is at  $R = R_0 \equiv 8.5 \text{ kpc}$ ,  $\theta_\odot = -180^\circ$  moving on a purely circular orbit with  $V_\odot = -220 \text{ km s}^{-1}$ . The polar angle  $\phi$  is measured from the plane in the direction of the  $z$ -axis such that  $\phi \equiv \tan^{-1}(z/R)$ . The cone opening angle is then  $\alpha = \pi - 2\phi_{\text{min}}$ . The value of  $\phi_{\text{min}}$  sets the boundary of the simulated cloud population close to the Galactic plane. Our goal is to understand the kinematics of the clouds; we do not attempt to simulate their spatial distribution in this paper.

The observed  $V_{\text{LSR}}$  of a cloud moving with pure radial velocity  $V_{\text{out}}$  can then be written as:

$$V_{\text{LSR}} = V_{\text{out}} [\sin(\phi) \sin(b) - \cos(\phi) \cos(b) \cos(\ell + \theta)] + V_{\odot} \sin(l) \cos(b) \quad . \quad (1)$$

The values from DiT18 of opening angle  $\alpha = 140^\circ$  and a constant  $V_{\text{out}} = 330 \text{ km s}^{-1}$  produce a  $|V_{\text{LSR}}|$  distribution shown in Figure 3. It does not reproduce the observed kinematic anomaly, as it has clouds around  $|V_{\text{LSR}}| = 300 \text{ km s}^{-1}$  at nearly all latitudes.

The data provide some basic limits on  $V_{\text{out}}$  and  $\phi_{\text{min}}$ . The outflow velocity must reach  $V_{\text{out}} \gtrsim 300 \text{ km s}^{-1}$  at some locations to allow for values of  $|V_{\text{LSR}}| \gtrsim 300 \text{ km s}^{-1}$  observed in the GBT data. Likewise, it is necessary that the angle  $\phi_{\text{min}} \lesssim 20^\circ$  or a number of the observed clouds will not lie within the boundaries of the cones. The Miller-Bregman shell model for the bubble volume actually implies  $\phi_{\text{min}} = 0^\circ$ , i.e., an isotropic stream of clouds emanating from the Galactic Center. In practice, because of confusion with other HI emission at low  $|b|$ , the exact value of  $\phi_{\text{min}}$  enters only weakly into the results, but simulations with  $\phi_{\text{min}} < 15^\circ$ , i.e., a cone opening angle  $\alpha > 150^\circ$ , would predict the existence of clouds whose kinematics are not consistent with the kinematic anomaly for reasonable values of  $V_{\text{out}}$ .

In the previous analyses, nearly identical values of  $\phi_{\text{min}}$  were found for the ATCA and GBT cloud samples (McG13; DiT18) so this is unlikely to be the source of the difference in their maximum  $|V_{\text{LSR}}|$ . We consider instead the case where the outflow velocity changes with distance from the Galactic Center,  $d$ . For simplicity, we consider models of the form

$$V_{\text{out}}(d) = \begin{cases} V_0 + (V_{\text{max}} - V_0) \frac{d}{d_{\text{acc}}} & \text{for } d < d_{\text{acc}} \\ V_{\text{max}} & \text{for } d \geq d_{\text{acc}} \end{cases} \quad (2)$$

where  $d$  is the distance from the Galactic Center and  $d_{\text{acc}}$  is the distance over which the outflow is accelerated from the minimum to the maximum value. Note that for a purely radial outflow whose magnitude depends on  $d$ , the outflow velocity at any  $|z|$  can vary considerably, especially at low  $|z|$ .

A set of simulations was run with varying parameters and compared with properties of the 196 known HI clouds. The simulations were evaluated on three criteria: 1) The parameters had to produce a distribution of  $V_{\text{LSR}}$  with  $|b|$  that reproduced the kinematic anomaly. 2) Most of the clouds in the ATCA and GBT surveys had to be consistent with the  $(\ell, b, V_{\text{LSR}})$  limits of the simulation. 3) At the  $(\ell, b)$  of each observed cloud, the

simulation had to produce a  $V_{\text{LSR}}$  within a few  $\text{km s}^{-1}$  of the observed  $V_{\text{LSR}}$  somewhere within the adopted Fermi Bubble boundaries. There was no attempt to match the distribution of the numbers of observed clouds in longitude or latitude, only their kinematics.

A selection of parameter combinations that produces acceptably good distributions is given in Table 3. These models can account for the kinematics of  $\gtrsim 95\%$  of the observed HI clouds as well as the components in the UV absorption spectra. Figure 6 shows detailed results for one set of parameters for comparison with Figure 2. We conclude that the simplest explanation for the kinematic anomaly of Fermi Bubble HI clouds observed at low  $|b|$  is an increase in  $V_{\text{out}}$  with distance from the Galactic Center.

We have explored simulations where the clouds arise from a region several hundred pc in size around the Galactic Center and not from a single point, but those still require acceleration to produce the kinematic anomaly. It is important to realize that the detected HI clouds extend to the limits of the areas covered by the ATCA and GBT surveys so the full extent of the cloud population in longitude and latitude is not known. The GASS survey does cover a much larger area, but we have found that it is not very good at detecting clouds such as those found by the GBT. This is most likely because its poorer angular resolution causes significant beam dilution of the 21cm line; it also has lower sensitivity. The current HI data thus do not place significant constraints on the size of the region that originates the clouds. A similar situation applies to the cloud acceleration. For simplicity, we have adopted a linear acceleration term because the data provide poor constraints on more complex (and more realistic) acceleration functions. More extensive observations are required.

## 6. DISCUSSION AND CONCLUSIONS

Although the simulations we use here are quite crude, they clearly imply that the clouds observed in the lower regions of the Fermi Bubbles must have been accelerated from  $\lesssim 200 \text{ km s}^{-1}$  to  $\approx 330 \text{ km s}^{-1}$  in their first few kpc of travel away from the Galactic Center. Using the kinematic model of Eq.2 we can estimate a location for every HI cloud in the ATCA and GBT catalogs. Virtually all lie at  $|z| < 1.5 \text{ kpc}$  at a distance  $d < 3 \text{ kpc}$  from the Galactic Center and have presumably been entrained in a hot wind that has a much higher expansion velocity. Components detected in UV spectra at  $b = -6^\circ.6$  and  $b = +11^\circ.2$  over a wide range of ionization stage (Fox et al. 2015; Savage et al. 2017) have kinematics consistent with those of the HI clouds.

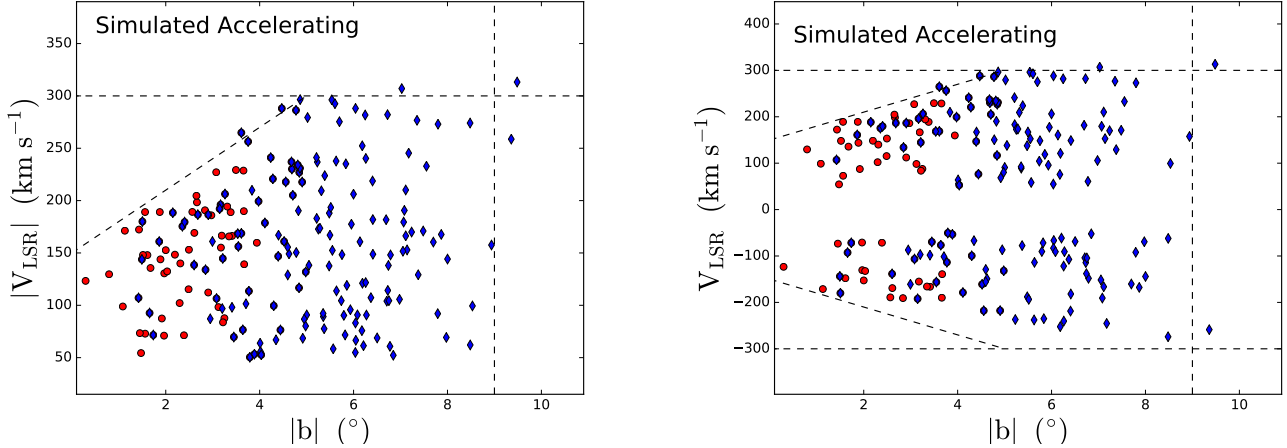


**Figure 6.** *Left panel:*  $|V_{\text{LSR}}|$  vs.  $|b|$  for a simulated population of clouds within the Fermi Bubbles with an opening angle  $\alpha = 145^\circ$  and  $V_{\text{out}}$  that varies linearly from  $175 \text{ km s}^{-1}$  at  $b = 0^\circ$  to  $330 \text{ km s}^{-1}$  for clouds 3.5 kpc from the Galactic Center (model 3 of Table 3). Red circles show clouds that appear in the regions covered only in the ATCA survey and blue diamonds show those that occur in regions covered by the GBT surveys. The dashed fiducial lines are identical to those in Figure 2, to which these figures should be compared. This simulation qualitatively matches the observations in that it reproduces the absence of clouds with  $|V_{\text{LSR}}| > 200 \text{ km s}^{-1}$  at  $|b| \lesssim 4^\circ$ . *Right panel:* Same as left panel, but for positive and negative velocity clouds plotted separately.

**Table 3.** Simulations that give acceptable agreement with the observations. The parameter  $\alpha$  is the cone opening angle; other parameters are defined in Eq. 1 and Eq. 2.

Model	$V_0$	$V_{\text{max}}$	$d_{\text{acc}}$	$\alpha$
	( $\text{km s}^{-1}$ )	( $\text{km s}^{-1}$ )	( $\text{km s}^{-1} \text{ kpc}^{-1}$ )	( $^\circ$ )
(1)	(2)	(3)	(4)	(5)
1	165	330	2.5	140
2	165	300	3.5	150
3	175	330	3.5	145
4	200	330	2.5	140

Observations, theoretical studies, and hydrodynamical simulations suggest that a hot wind can accelerate compact, cold gas clouds such as we observe in the 21cm line (e.g., Castor et al. 1975; Veilleux et al. 2005; Cooper et al. 2008). In the so-called “entrainment” scenario, cold gas is hit by the hot flow and dragged until it is either shredded or approaches the velocity of the hot gas. The details of such a process are still unclear and very debated. Many high-resolution simulations of cold gas clouds in hot flows have shown that entrainment is a highly destructive process, the cold gas being ripped and ionized on time-scales much shorter than needed to reach the observed velocities of hundreds of  $\text{km s}^{-1}$  (e.g.

Scannapieco & Brüggen 2015; Schneider & Robertson 2017; Sparre et al. 2019). In fact, when the density of the cold gas is much higher than the density of the hot gas, the cloud-crushing time  $t_{\text{cc}}$ , which governs the destruction timescale, is always much lower than the acceleration time  $t_{\text{acc}}$  because of the drag force, i.e.  $t_{\text{cc}} \ll t_{\text{acc}}$ . However, some studies suggest that a cloud lifetime can be prolonged through radiative cooling (Gronke & Oh 2018), thermal conduction (Brüggen & Scannapieco 2016) and magnetic fields (McCourt et al. 2015).

The kinematic model we use to explore  $V_{\text{LSR}}$  can also be used to estimate cloud lifetimes, though the form of the acceleration is not well constrained by our data.



Whereas we assume a linear acceleration, in an entrainment scenario acceleration is expected to be more violent (e.g., Zhang et al. 2017). Nonetheless, our values for  $V_0$  and  $V_{\max}$  give estimated cloud lifetimes slightly longer than those calculated with a constant outflow velocity by DiT18 and range from 4 Myr to 10 Myr, with a median of 6.5 Myr. These longer lifetimes add an additional challenge to the entrainment scenario.

While the 200 HI clouds that we study here appear to be part of a single population whose kinematics can be described quite simply, there is certainly the possibility that the Galactic nucleus undergoes periodic outbursts (e.g., Veilleux et al. 2005; Bland-Hawthorn et al. 2019) leaving other anomalous-velocity gas as its mark on the interstellar medium. This might explain the anomalous high-velocity absorption observed toward the Galactic center at very high latitudes (Bordoloi et al. 2017; Karim et al. 2018) whose kinematics is not consistent with the outflow described here.

As is evident in Figure 1, only a fraction of the volume of the Fermi Bubbles has been searched for HI clouds to the sensitivity levels needed to detect the objects described here and to follow their evolution in space. We are continuing our 21cm HI observational program with the GBT to further refine the properties of this

population. Additional measurements of UV absorption spectra through the Fermi Bubbles in the range  $10^\circ \leq |b| \leq 30^\circ$  would supply critical information.

## ACKNOWLEDGMENTS

Observations were made with the Green Bank Telescope under proposal 19A.337. The Green Bank Observatory is a facility of the National Science Foundation, operated under a cooperative agreement by Associated Universities, Inc. We acknowledge the support of the Australian Research Council (ARC) through grant DP160100723. N.M.-G. acknowledges the support of the ARC through Future Fellowship FT150100024.

*Facilities:* ATCA, GBT, Parkes

*Software:* <sup>3D</sup>BAROLO (Di Teodoro & Fraternali 2015), GBTGRIDDER, GBTIDL, MIRIAD (Sault, Teuben, & Wright 1995).

## REFERENCES

- Binney, J., Gerhard, O. E., Stark, A. A., Bally, J., & Uchida, K. I. 1991, MNRAS, 252, 210, doi: [10.1093/mnras/252.2.210](https://doi.org/10.1093/mnras/252.2.210)
- Bland-Hawthorn, J., & Cohen, M. 2003, ApJ, 582, 246, doi: [10.1086/344573](https://doi.org/10.1086/344573)
- Bland-Hawthorn, J., Maloney, P., Sutherland, R., et al. 2019, arXiv e-prints, arXiv:1910.02225. <https://arxiv.org/abs/1910.02225>
- Boothroyd, A. I., Blagrove, K., Lockman, F. J., et al. 2011, A&A, 536, A81, doi: [10.1051/0004-6361/201117656](https://doi.org/10.1051/0004-6361/201117656)
- Bordoloi, R., Fox, A. J., Lockman, F. J., et al. 2017, ApJ, 834, 191, doi: [10.3847/1538-4357/834/2/191](https://doi.org/10.3847/1538-4357/834/2/191)
- Brüggen, M., & Scannapieco, E. 2016, ApJ, 822, 31, doi: [10.3847/0004-637X/822/1/31](https://doi.org/10.3847/0004-637X/822/1/31)
- Burton, W. B., & Liszt, H. S. 1978, ApJ, 225, 815, doi: [10.1086/156547](https://doi.org/10.1086/156547)
- Carretti, E., Crocker, R. M., Staveley-Smith, L., et al. 2013, Nature, 493, 66, doi: [10.1038/nature11734](https://doi.org/10.1038/nature11734)
- Castor, J., McCray, R., & Weaver, R. 1975, ApJL, 200, L107, doi: [10.1086/181908](https://doi.org/10.1086/181908)
- Cooper, J. L., Bicknell, G. V., Sutherland, R. S., & Bland-Hawthorn, J. 2008, ApJ, 674, 157, doi: [10.1086/524918](https://doi.org/10.1086/524918)
- Di Teodoro, E. M., & Fraternali, F. 2015, MNRAS, 451, 3021, doi: [10.1093/mnras/stv1213](https://doi.org/10.1093/mnras/stv1213)
- Di Teodoro, E. M., McClure-Griffiths, N. M., Lockman, F. J., et al. 2018, ApJ, 855, 33, doi: [10.3847/1538-4357/aaad6a](https://doi.org/10.3847/1538-4357/aaad6a)
- Dobler, G., & Finkbeiner, D. P. 2008, ApJ, 680, 1222, doi: [10.1086/587862](https://doi.org/10.1086/587862)
- Fox, A. J., Bordoloi, R., Sav age, B. D., et al. 2015, ApJL, 799, L7, doi: [10.1088/2041-8205/799/1/L7](https://doi.org/10.1088/2041-8205/799/1/L7)
- Gronke, M., & Oh, S. P. 2018, MNRAS, 480, L111, doi: [10.1093/mnrasl/sly131](https://doi.org/10.1093/mnrasl/sly131)
- Kalberla, P. M. W., McClure-Griffiths, N. M., Pisano, D. J., et al. 2010, A&A, 521, A17, doi: [10.1051/0004-6361/200913979](https://doi.org/10.1051/0004-6361/200913979)
- Karim, M. T., Fox, A. J., Jenkins, E. B., et al. 2018, ApJ, 860, 98, doi: [10.3847/1538-4357/aac167](https://doi.org/10.3847/1538-4357/aac167)
- Kataoka, J., Tahara, M., Totani, T., et al. 2013, ApJ, 779, 57, doi: [10.1088/0004-637X/779/1/57](https://doi.org/10.1088/0004-637X/779/1/57)
- Keeney, B. A., Danforth, C. W., Stocke, J. T., et al. 2006, ApJ, 646, 951, doi: [10.1086/505128](https://doi.org/10.1086/505128)
- Lockman, F. J. 1984, ApJ, 283, 90, doi: [10.1086/162277](https://doi.org/10.1086/162277)
- Lockman, F. J., & McClure-Griffiths, N. M. 2016, ApJ, 826, 215, doi: [10.3847/0004-637X/826/2/215](https://doi.org/10.3847/0004-637X/826/2/215)

- McClure-Griffiths, N. M., Green, J. A., Hill, A. S., et al. 2013, *ApJL*, 770, L4, doi: [10.1088/2041-8205/770/1/L4](https://doi.org/10.1088/2041-8205/770/1/L4)
- McClure-Griffiths, N. M., Pisano, D. J., Calabretta, M. R., et al. 2009, *ApJS*, 181, 398, doi: [10.1088/0067-0049/181/2/398](https://doi.org/10.1088/0067-0049/181/2/398)
- McCourt, M., O’Leary, R. M., Madigan, A.-M., & Quataert, E. 2015, *MNRAS*, 449, 2, doi: [10.1093/mnras/stv355](https://doi.org/10.1093/mnras/stv355)
- Miller, M. J., & Bregman, J. N. 2016, *ApJ*, 829, 9, doi: [10.3847/0004-637X/829/1/9](https://doi.org/10.3847/0004-637X/829/1/9)
- Oort, J. H. 1977, *ARA&A*, 15, 295, doi: [10.1146/annurev.aa.15.090177.001455](https://doi.org/10.1146/annurev.aa.15.090177.001455)
- Sault, R. J., Teuben, P. J., & Wright, M. C. H. 1995, in *Astronomical Society of the Pacific Conference Series*, Vol. 77, *Astronomical Data Analysis Software and Systems IV*, ed. R. A. Shaw, H. E. Payne, & J. J. E. Hayes, 433
- Savage, B. D., Kim, T.-S., Fox, A. J., et al. 2017, *ApJS*, 232, 25, doi: [10.3847/1538-4365/aa8f4c](https://doi.org/10.3847/1538-4365/aa8f4c)
- Scannapieco, E., & Brüggen, M. 2015, *ApJ*, 805, 158, doi: [10.1088/0004-637X/805/2/158](https://doi.org/10.1088/0004-637X/805/2/158)
- Schneider, E. E., & Robertson, B. E. 2017, *ApJ*, 834, 144, doi: [10.3847/1538-4357/834/2/144](https://doi.org/10.3847/1538-4357/834/2/144)
- Sparre, M., Pfrommer, C., & Vogelsberger, M. 2019, *MNRAS*, 482, 5401, doi: [10.1093/mnras/sty3063](https://doi.org/10.1093/mnras/sty3063)
- Su, M., Slatyer, T. R., & Finkbeiner, D. P. 2010, *ApJ*, 724, 1044, doi: [10.1088/0004-637X/724/2/1044](https://doi.org/10.1088/0004-637X/724/2/1044)
- Veilleux, S., Cecil, G., & Bland-Hawthorn, J. 2005, *ARA&A*, 43, 769, doi: [10.1146/annurev.astro.43.072103.150610](https://doi.org/10.1146/annurev.astro.43.072103.150610)
- Zhang, D., Thompson, T. A., Quataert, E., & Murray, N. 2017, *MNRAS*, 468, 4801, doi: [10.1093/mnras/stx822](https://doi.org/10.1093/mnras/stx822)

## APPENDIX

## A. GBT OBSERVATIONS AND DATA REDUCTION

Observations of the 21 cm line were made with the Robert C. Byrd Green Bank Telescope (GBT) of the Green Bank Observatory that has an angular resolution of 9/1 at 1.4 GHz. The GBT L-band receiver used for these measurements has a system temperature on cold sky of 18 K, although at low latitudes near the Galactic Center nonthermal continuum emission increases the system temperature significantly in some directions. Spectra were taken using in-band frequency-switching which gave a clean spectral response over  $\pm 656 \text{ km s}^{-1}$  at a channel spacing of  $0.15 \text{ km s}^{-1}$ . Maps were made on-the-fly scanning in Galactic longitude at a fixed latitude. The region between  $0^\circ \leq \ell \leq 6^\circ$ ,  $+1^\circ \leq b \leq +3^\circ$  was covered in 3 patches, each  $2^\circ \times 2^\circ$ . Each patch was observed several times to reduce the noise level for a total integration time of 46 hours over the 12 square degree field.

Spectra were calibrated, smoothed to  $1.06 \text{ km s}^{-1}$  velocity resolution, and corrected for stray radiation using the procedure described by [Boothroyd et al. \(2011\)](#), and a third degree polynomial was fit to emission-free regions of each spectrum.

All of the clouds first detected over this region in the ATCA survey were present in the new GBT data. In addition, the cloud-finding algorithm described in [DiT18](#) isolated four new clouds, whose properties are listed in [Table 2](#). Although the newly-detected clouds all have negative velocities this does not seem to be the result of any bias. When all clouds in this area are included, nine have negative and 12 have positive velocities.